IJNRD.ORG ISSN : 2456-4184
INTERNATIONAL JOURNAL OF NOVEL RESEARCH AND DEVELOPMENT (IJNRD) | IJNRD.ORG
An International Open Access, Peer-reviewed, Refereed Journal

Study of Structural, Electronic Structure and Optical Properties of the $Zn_{0.97}Cu_{0.03}O$ Nanoparticles Sample Synthesized by Co-precipitation Method

[1]Mahendra Kumar Gora, [2]Arvind Kumar, [3]Subhash Chandra, [4]Sanjay Kumar

[1234]Assistant Professor
[1234]Department of Physics,
University of Rajasthan, Jaipur (Rajasthan), India-302004

Abstract: 3% Copper-doped Zinc Oxide nanoparticles (i.e., $Zn_{0.97}Cu_{0.03}O$) have been prepared through the co-precipitation technique. The synthesized nanocrystalline sample has been investigated utilizing X-ray diffraction (XRD), UV–visible, Photoluminescence (PL) spectroscopy, Scanning Electron Microscopy (SEM), and X-ray photoelectron spectroscopy (XPS). The lattice parameters and detailed crystallographic investigation were analyzed using Rietveld refinement. The synthesized sample's XRD patterns confirmed the average crystalline size between 40 and 62 nm and the hexagonal wurtzite crystal structure of the $P6_3mc$ space group. SEM images have been utilized to analyze the morphology; they show an agglomerated oval-shaped particle structure and an uneven grain size distribution. The prepared nanoparticles' average particle size observed by SEM micrographs and the values determined by XRD patterns match quite well. The XPS findings exhibited oxygen vacancies (V_o) in the synthesized specimen. In consent with the XPS consequences, PL outcomes confirm the appearance of defects-related states and V_o's. According to UV-visible spectroscopy results, the band gap (E_g) of made nanoparticles of the $Zn_{0.97}Cu_{0.03}O$ has been found to be 3.28 eV.

IndexTerms - XPS, Rietveld Refinement, PL, Spintronics, DMSs.

I. INTRODUCTION

Different transition metal (TM) doped semiconductor metal oxides have piqued the researchers' curiosity. Such semiconductors are called diluted magnetic semiconductors (DMSs), and their prospective uses in spintronics devices have garnered considerable interest in this field of research [1]. Because III-V type semiconductors are moderately soluble in TM, most previous work on DMSs has focused on them [2, 3]. Zinc oxide (ZnO), a semiconductor metal oxide of the II-VI type, has garnered significant attention as a DMS due to its enormous near 60 meV exciton binding energy and broad near about 3.37 eV band gap [4]. It is desired to develop an effective, economical, and reproducible method for producing DMSs on an enormous scale for practical applications. By using spintronic devices, it is possible to combine the information-storing capabilities of magnetic components with logic semiconductors in a single material [5, 6]. Zinc Oxide substituted with 3d TM (e.g., Mn [7, 8], Co [9], Cu [10], Ni [11], and Cr [12]) has thus been thoroughly explored kind of a hopeful DMS for potential uses in spintronic devices. The Cu-substituted ZnO tantra has drawn considerable notice because of the potential for low formation energy caused by the radius match-up of Zn and Cu ions [13].

A promising semiconductor material, Zinc Oxide finds application in solar cells, photodiodes, gas sensors, photo-detectors, piezoelectric transducers, UV-light emitting diodes (UV-LEDs), transparent conductive oxides, and optical and magnetic devices because of its broad direct band gap and high exciton binding energy at 300 K [14, 15, 16, 17, 18]. Because of inherent flaws such as interstitial atoms and oxygen vacancies, it functions as an n-type semiconductor under ordinary circumstances [19, 20]. Numerous techniques, including auto-combustion [21], hydrothermal [22], ball-milling [23], co-precipitation, and sol-gel [24], are frequently used to synthesize ZnO nanoparticles. The co-precipitation technique is recommended because it is inexpensive and enables homogeneity control. Furthermore, this is a reasonably easy procedure for

preparing Cu-doped ZnO nanoparticles. Additionally, research has shown that doping ZnO with elements like Al [25], Fe [26], Mn [27], Co [28, 29], and Cu [30] can be changed its electrical, magnetic, and optical characteristics. The Cu dopant is very appealing because of its similar physical and chemical characteristics to Zn and low resistivity [31]. Therefore, it may be applied to enhance ZnO's optical and electrical conductivity.

Cu incorporation is said to impact the number of charge carriers and decrease the band gap, greatly enhancing ZnO's electrical conductivity at room temperature [18, 32]. According to some studies, doping of Cu into the ZnO thin films introduced multiple V_o;s, which played an essential role in altering the electric and optical properties [30]. Some studies have also explored the ZnO nanoparticle's structural and optical characteristics [33, 34]. Additionally, nanoparticles offer an exceptional platform for producing many oxygen vacancies ($V_{O's}$) necessary to generate ferromagnetism and change the band gap. Thus, nanoparticles magnetism and band gap change are considered hopeful research areas

In the current study, we prepared the $Zn_{0.97}Cu_{0.03}O$ nanoparticles through co-precipitation to study their structural, electronic, and optical characteristics. We used X-ray diffraction (XRD) to investigate the synthesized nanoparticle's structural properties. X-ray electron spectroscopy has been applied to examine the sample's electronic structure. UV-visible and PL spectroscopy have been utilized to investigate the optical characteristics of the synthesized nanoparticles.

II. SAMPLE SYNTHESIS

$Zn_{0.97}Cu_{0.03}O$ nanoparticles sample was prepared using the co-precipitation method. The primary materials used to synthesize the sample were high-purity analytical-grade Zinc Acetate dihydrate, Copper Acetate monohydrate, and Potassium Hydroxide (Make; Sigma-Aldrich). Deionized water was used to dissolve the stoichiometric amounts of all reactants and make an aqueous solution. The mixture was continually stirred and heated to 60 ºC. 1 M solution of KOH has been spilled drop by drop while constantly stirring to keep pH at roughly 10. The solution was kept at 90 ºC for five minutes while being constantly stirred. It was then allowed to drop to room temperature while being continuously stirred and heated to 90 ºC once more. 5 ml of oleic acid has been added to the mixture as a surfactant at 90 ºC. The mixture was gradually cooled until it reached room temperature with constant stirring. A couple of drops of HNO_3 have been poured to achieve a pH of 7. Acetone and hot deionized water were used to clean the residue. The precipitate has been dried on a hot plate at 60 ºC for three hours. The dried powder has been annealed in an electric furnace for three hours at 300 ºC. Various techniques were used to characterize the different properties of the prepared powder sample of the nanoparticles.

III. CHARACERIZATION TECHNIQUES

The XRD patterns were obtained for structural and phase purity analysis using the diffractometer (Panalytical: X'Pert PRO), which utilizes the line source Cu-K_α with wavelength (λ) ≈ 1.5406 A˚. XPS has been used to identify and evaluate the chemical state of the constituent elements. PL spectrum has been employed to explore defect-related characteristics and assess the vacancies in the prepared sample. The PL spectra were taken within the 350 nm to 650 nm wavelength range at 300 K using a fluorescence spectrophotometer with an excitation wavelength of 300 nm. UV-vis. absorption spectrum has been applied to investigate the band gap of the formed specimen. Absorption spectrum have been recorded in the 200 to 800 nm wavelength range using a UV-visible spectrometer at 300 K.

IV. RESULTS AND DISCUSSION

4.1. XRD Investigation

The phase and crystal structures of the synthesized sample have been examined using XRD. Using the FP-Suite-TB software, the Rietveld refinement analysis of the XRD peaks was performed to determine the detailed crystal structure of the sample. Fig. 1 demonstrates the XRD pattern of the prepared $Zn_{0.97}Cu_{0.03}O$ nanoparticles specimen. The synthesized material's XRD peaks are consistent with a wurtzite-type ZnO crystal structure (JCPDS card no. 36-1451) [13, 35]. The XRD of $Zn_{0.97}Cu_{0.03}O$ nanoparticles, with peaks commensurate to the (100), (002), (101), (102), (110), (103), (200), (112), and (201) planes, indicates the existence of ZnO phase, which ascribed to a wurtzite crystal structure [13, 35]. This pattern does not indicate any other CuO, Cu, or binary Zn-Cu phase peaks. Fig. 2 indicates Rietveld refinement of a prepared sample of nanoparticles. The specimen diffractogram consists of two overlapping sets: the simulated counterpart (Rwp) from Rietveld refinement, shown with circles, and experimental data (Rexp), shown with solid lines. Cyan-colored lines on the bottom indicate differences among the simulated outcomes of the Rietveld analysis and the experimental data [13].

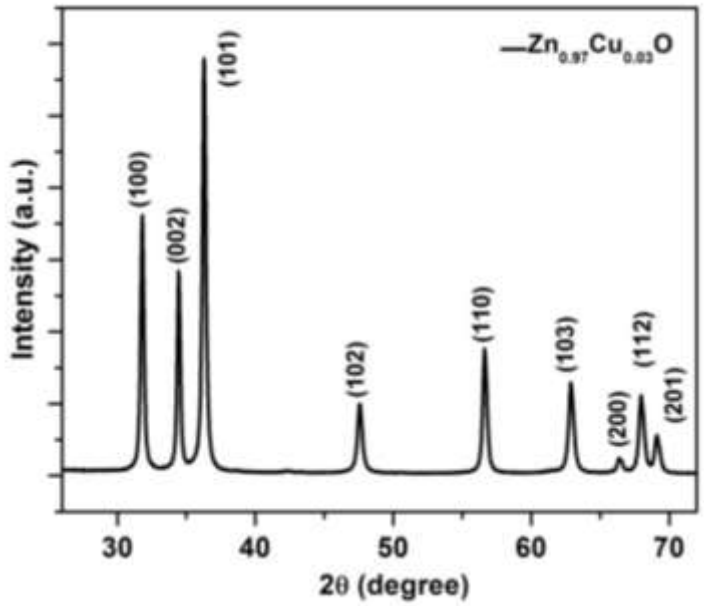

Fig.1: XRD peaks of the $Zn_{0.97}Cu_{0.03}O$ sample.

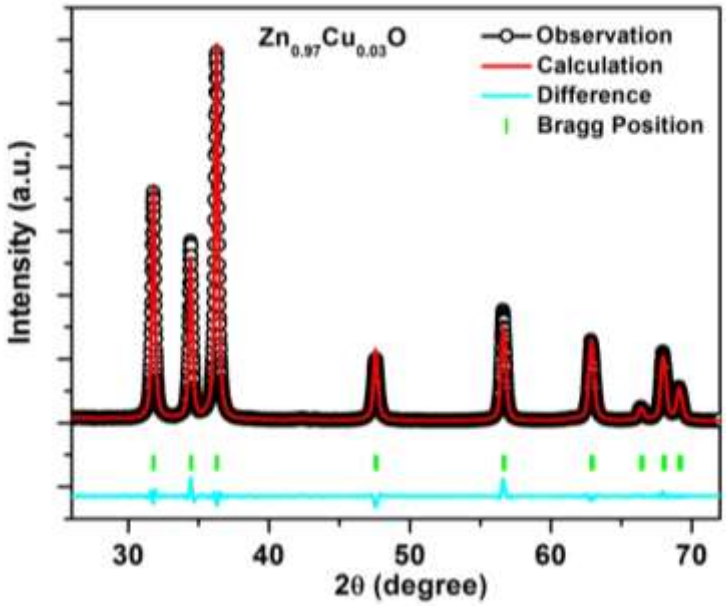

Fig.2: Rietveld refinement of the prepared $Zn_{0.97}Cu_{0.03}O$ sample.

The $Zn_{0.97}Cu_{0.03}O$ sample's Rexp and Rwp values are 1.9 and 1.3, respectively, and the Chi-squared value (X^2) has been found near about 3.07. The low X^2 and R factors values propose that refinements are comparatively credible [36].

The wurtzite structure of the $P6_3mc$ space group, which has atomic positions of (1/3, 2/3, 0.3817) for O and (1/3, 2/3, 0) for Zn, is consistent with all of the diffraction peaks for the $Zn_{0.97}Cu_{0.03}O$ nanoparticles [37]. The lattice parameters a and c, as determined by the Rietveld refinement analyses, have been found to have values of 3.2496 Å and 5.2072 Å, respectively, for the prepared sample. Cu doping has been found to alter the lattice size because of the ionic size variations among Cu ($Cu^{2+}\approx$ 0.57 Å) and Zn ($Zn^{2+}\approx$ 0.60 Å) ions with the similar coordination number [38]. Others have also reported an achievable lattice contraction because of the doping of Cu in the ZnO matrix [39, 40].

The prepared nanoparticles' average crystallite size has been calculated using the Scherrer formula below.

$$D = \frac{0.9\lambda}{\beta \cos\theta}$$

In this case, D stands for crystallite size, λ for X-ray radiation wavelength, θ for diffraction angle, and β for full width at half maximum (FWHM) [41]. The synthesized samples' crystallite size has been found within the 40 to 62 nm range. The value of c/a, determined to be 1.6, indicates an optimally closed-packed hexagonal configuration [42].

4.2. SEM Analysis

SEM micrographs have been utilized to examine the size, shape, and surface morphology of the $Zn_{0.97}Cu_{0.03}O$ nanoparticles' grains or particles. Fig. 3 displays SEM images of the formed $Zn_{0.97}Cu_{0.03}O$ sample. Fig. 3 depicts the surface

morphology of the formed sample, which has an agglomerated oval-shaped particle structure and an uneven grain size distribution. Most of the particles are between 40 and 62 nm in size. As a result, the average particle size of nanoparticles, as determined from the XRD patterns, corresponds nicely with the results seen in the SEM images.

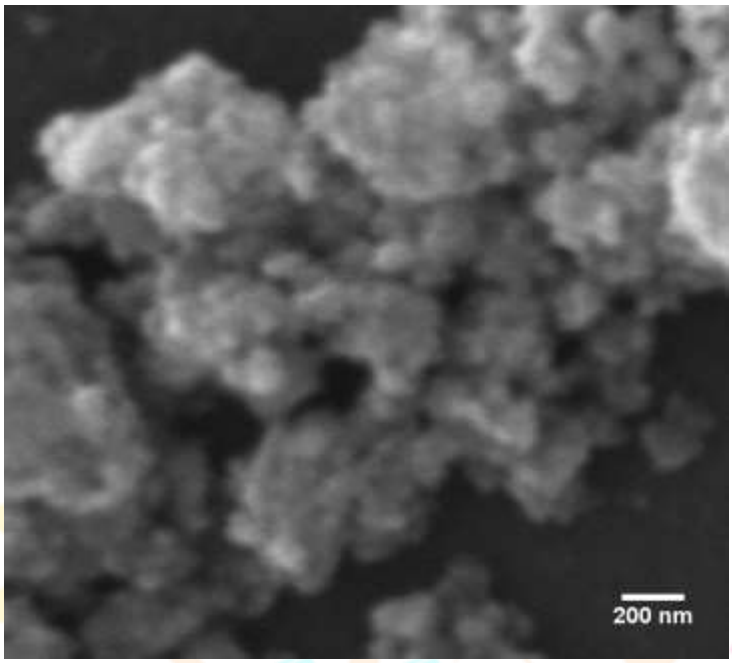

Fig.3: SEM image of $Zn_{0.97}Cu_{0.03}O$ nanoparticles sample.

4.3. XPS analysis

XPS analyses investigated the constituents' chemical composition and state of $Zn_{0.97}Cu_{0.03}O$ nanoparticles. The C*1s* signal (284.8 eV) has been standardized for the charge and binding energy modifications. Fig. 4 shows the survey spectra of $Zn_{0.97}Cu_{0.03}O$ nanoparticles. In the prepared nanoparticles sample, the elements Zn, O, Cu, and C were identified as having the strongest signals in the XPS survey spectrum; no signal for any other element was found. Fig. 5 displays the characteristics of the Zn*2p* signal for the synthesized sample. Zn$2p_{3/2}$ and Zn$2p_{1/2}$ peaks, arising from high spin-orbit coupling, have been found for $Zn_{0.97}Cu_{0.03}O$ nanoparticles at 1022.28 and 1045.30 eV, respectively. These binding energy observations agree with previously demonstrated binding energy values for ZnO [43]. The energy separation among the Zn$2p_{3/2}$ and Zn$2p_{1/2}$ peaks is 23 eV, compatible with the earlier stated values [44]. It indicates the chemical environment of Zn^{2+} is unaffected by the doping of Cu^{2+} into the ZnO matrix.

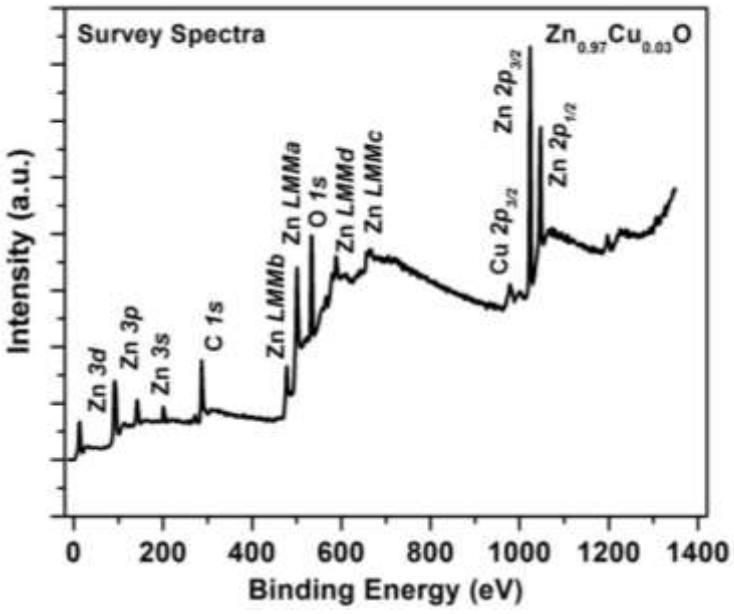

Fig.4: XPS survey spectra of the $Zn_{0.97}Cu_{0.03}O$ sample.

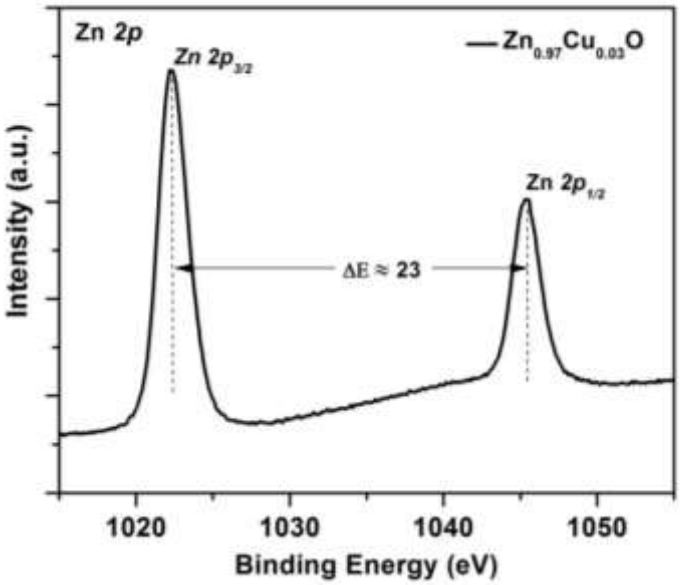

Fig.5: High-resolution XPS Zn2*p* spectrum of $Zn_{0.97}Cu_{0.03}O$ nanoparticles.

Multicomponent oxygen species are present at the surfaces of the prepared sample, as revealed by the asymmetric structure of the O*1s* XPS spectrum displayed in Fig. 6 [45]. Three Gaussian peaks have been fitted to the synthesized nanocrystalline sample's O*1s* XPS spectra, as shown in Fig. 7.

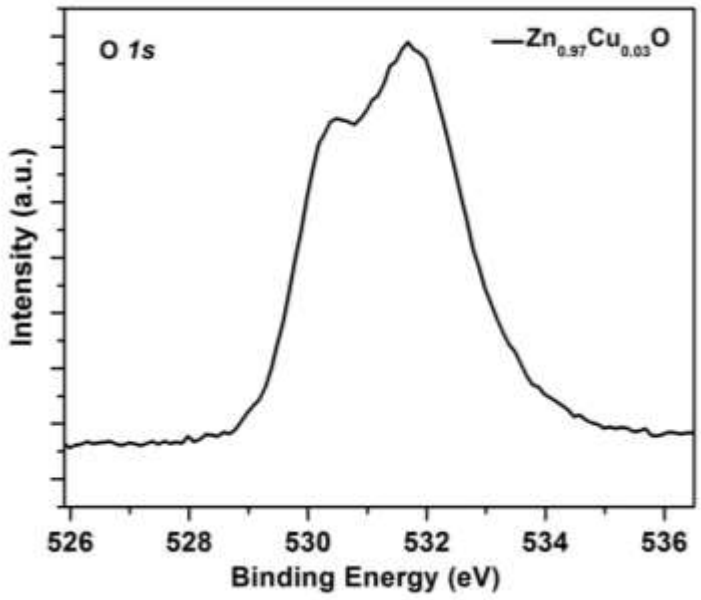

Fig.6: O*1s* high-resolution XPS spectrum of the $Zn_{0.97}Cu_{0.03}O$ nanoparticles.

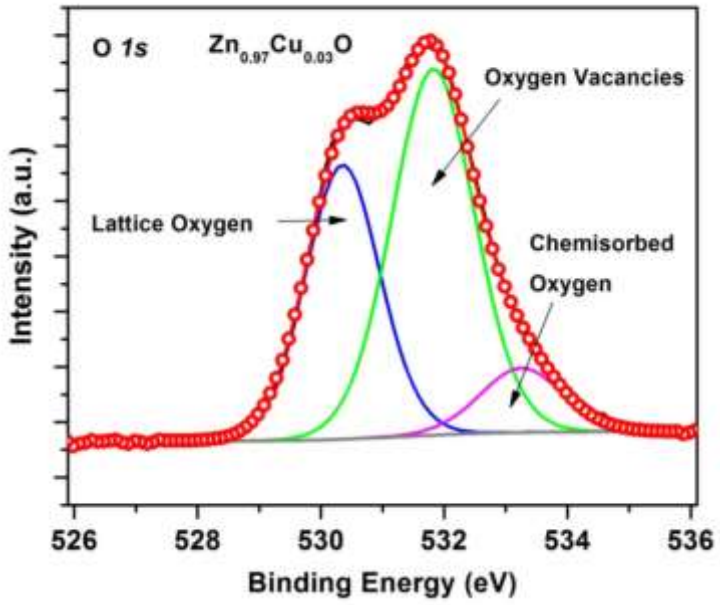

Fig.7: Three Gaussian peaks fitted in the O*1s* XPS spectrum of the $Zn_{0.97}Cu_{0.03}O$ sample.

Fig. 7 shows the three deconvoluted O*1s* peaks in the $Zn_{0.97}Cu_{0.03}O$ nanoparticles, detected at the binding energies of 530.35 eV, 531.82 eV, and 533.12 eV. These peaks are designated in the following manner. Due to the presence of lattice oxygen in the structure of ZnO, the lower binding energy peak is induced, and the middle peak originates from the presence of V_o's in the ZnO lattice [35]. Adsorbed oxygen molecules (OH^-, adsorbed H_2O, and chemisorbed oxygen) on nanocrystals' surfaces cause a higher binding energy peak [35, 46]. These results show the oxygen vacancies in the synthesized $Zn_{0.97}Cu_{0.03}O$ nanocrystalline sample.

The XPS spectrum of the Cu*2p* peaks for the $Zn_{0.97}Cu_{0.03}O$ sample is displayed in Fig. 8. The two broad peaks, $2p_{3/2}$ and $2p_{1/2}$, in Cu*2p* spectra originate from spin-orbit splitting of the Cu*2p* states.

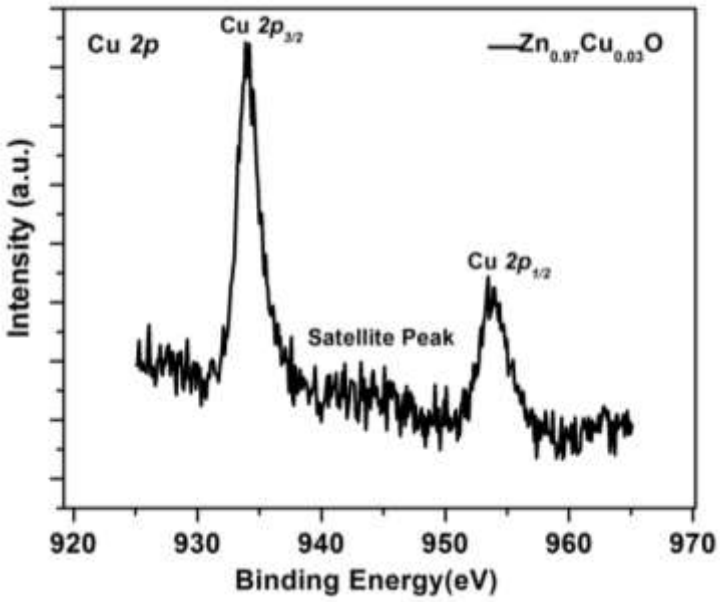

Fig.7: XPS Cu*2p* spectrum of the $Zn_{0.97}Cu_{0.03}O$ sample.

The Cu$2p_{3/2}$ and Cu$2p_{1/2}$ peaks are detected in the prepared sample at 933.92 eV and 953.96 eV, respectively. The spin-orbit doublet splitting of the Cu$2p_{3/2}$ and Cu$2p_{1/2}$ peaks have a binding energy separation of 20 eV [43]. Furthermore, satellite peaks in the sample are detected at 944.05 eV. These properties are because of the divalent state of Cu ions in the ZnO matrix [47].

4. 4. Optical properties

4.4.1. Photoluminescence studies

The $Zn_{0.97}Cu_{0.03}O$ nanoparticles' structural flaws have been examined using PL spectroscopy. At room temperature, PL spectra have been taken at an excitation wavelength of 300 nm, and they are displayed in Fig. 8 for prepared samples. It is found that PL spectra of the synthesized sample exhibit the emission regions (bands) listed below: (i) Ultra-violet, (ii) Violet, (iii) Blue, (iv) Green, (v) Yellow and (vi) Orange emission [48]; all these regions are depicted in Fig. 8.

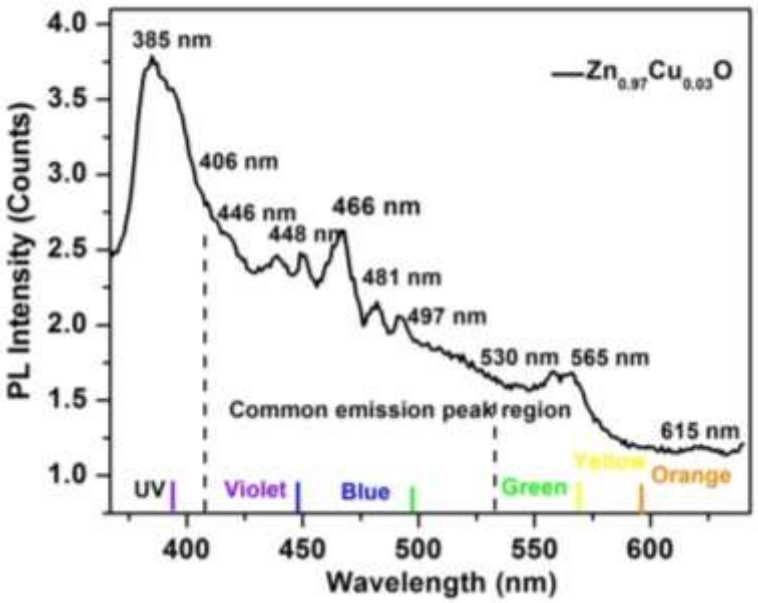

Fig.8: PL spectra of the $Zn_{0.97}Cu_{0.03}O$ sample.

At 385 nm, the UV peak related to near-band emission (NBE) was observed, possibly caused by free excitons recombination [49]. Three peaks have been detected in the violet zone. The first peak, generated by a transition among Zinc interstitials (Zni) and the valence band of ZnO, was detected at 406 nm [50]. The remaining two peaks, the second found at 446 nm, are attributable to the migration from the bottom layer of the conduction band ($E_{c)}$ to Zinc vacancy (Zn_v), and third at 448 nm, because of the movement of electrons from the Zn_i condition to the top of the valence band (E_v) [51]. Defect luminescence or deep-level emission; generated by V_o, is responsible for the blue discharge peaks (blue radiation region) detected at 448 nm and 466 nm in the sample [52, 53]. The transfer from the shallow donor level of the Zn_i to the E_v band is responsible for the peak at 481 nm [49]. Due to the presence of V_o on the ZnO surface, two peaks appeared in the green region, one at 497 nm and the other at 530 nm [54]. Transition among the flabbily captured electron and the firmly captured hole in the singly ionized V_o^+ is responsible for the peak observed at 525 nm in green emission and 615 nm in orange emission [55]. These results show that oxygen vacancies are present in the synthesized sample of $Zn_{0.97}Cu_{0.03}O$ nanoparticles and are in apparent concurrence with the XPS findings.

4. 4.2. UV visible Spectroscopy

As displayed in Fig. 9, UV-vis. absorption spectrum for the $Zn_{0.97}Cu_{0.03}O$ sample that measurements taken at 300 and 800 nm wavelengths show a distinct peak in the UV area. Absorption edge of the $Zn_{0.97}Cu_{0.03}O$ nanocrystalline specimen has been observed at 376 nm.

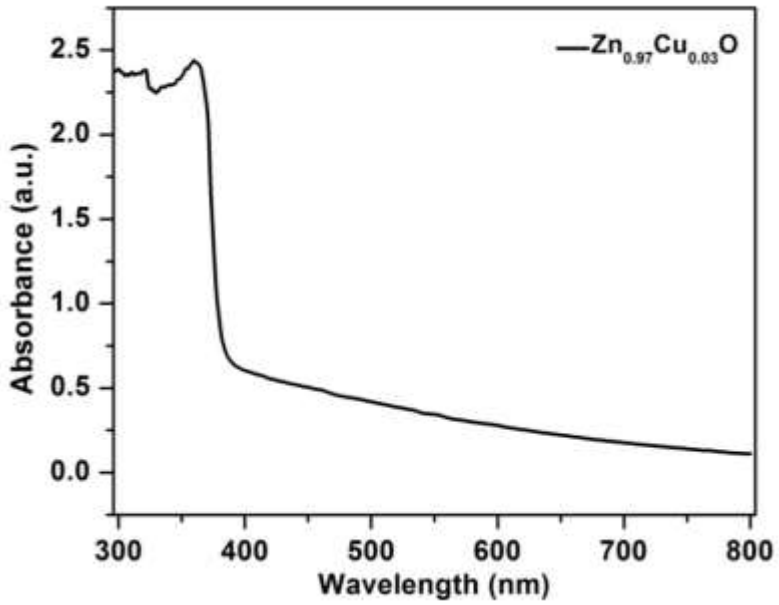

Fig.9: The UV-vis. absorption spectrum of the $Zn_{0.97}Cu_{0.03}O$ sample.

Tauc's equation, which describes the link among incident photon energy and the semiconductors' absorption coefficient, has been utilized to estimate the optical band gap of the nanocrystalline material formed. Tauc's equations [56]:

$$\alpha h\upsilon = A\ (h\upsilon - Eg)^n$$

In this equation, an exponent n is 1/2 for the direct band gap, A is a constant, Eg is the semiconductor material's band gap, h is the Planck constant, and α is the absorption coefficient.

The Tauc plot of the synthesized sample is displayed in Fig.10. The band gap (E_g) for the $Zn_{0.97}Cu_{0.03}O$ nanoparticles is obtained through plotting a $(\alpha h\upsilon)^2$ versus photon energy ($h\upsilon$) graph and expanding this plot's straight-line section to the $h\upsilon$ axis. The value of Eg obtained for the $Zn_{0.97}Cu_{0.03}O$ sample is 3.28 eV.

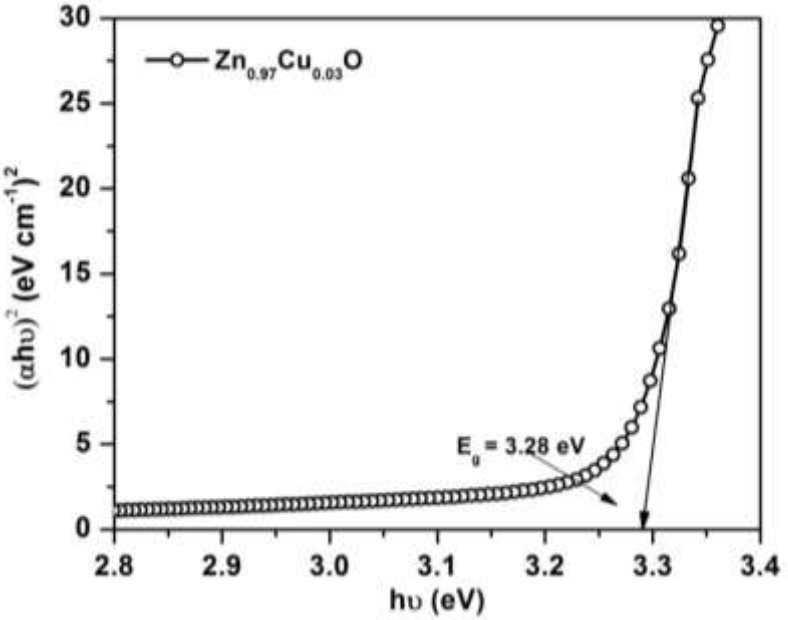

Fig.10: Tauc plot for the $Zn_{0.97}Cu_{0.03}O$ nanoparticles.

Similar results were found by Bhardwaj et al., who attributed the band gap's decrease to the prominent flaw levels found in the Cu-substituted ZnO nanoparticles [57]. Energy gap is frequently altered by changes in the size and structure of the substance as well as the density of defects brought on by the impurity atoms [58]. An inversely proportional relationship is typically present between the energy band gap and crystallite size [59].

V. Conclusions

The 3% Cu-doped ZnO (i.e., $Zn_{0.97}Cu_{0.03}O$) nanocrystalline sample was synthesized by the co-precipitation technique. Their structural, electronic, and optical properties have been studied. The outcomes showed that Cu doping happens through the substitution illation of Cu^{2+} ions in the ZnO matrix, as displayed from a comprehensive crystallographic investigation by the Rietveld refinement of the XRD data. The band gap (E_g) of the prepared sample has been calculated by the UV visible spectroscopy outcomes, indicating that the obtained value of Eg was 3.28 eV. The present work depicts a correlation among the crystal and electronic structure, band gap, and optical characteristics of the made $Zn_{0.97}Cu_{0.03}O$ nanoparticles. XPS and PL results show the presence of V_o's and defect level states in the synthesized sample. This co-precipitation approach is economic, easy, and fast doping that can be acclimated to variant TM elements to acquire DMS with optical properties.

.

References

[1] Wolf, S.A., Awschalom, D.D., Buhrman, R.A., Daughton, J.M., Molnar, S.V., Roukes, M.L., Chtchelkanova, A.Y. and Treger, D.M. 2001. Spintronics: a spin-based electronics vision for the future. Science, 294: 1488-1495.

[2] Koshihara, S., Oiwa, A., Hirasawa, M., Katsumoto, S., Iye, Y., Urano, C., Takagi, H. and Munekata, H. 1997. Ferromagnetic order induced by photogenerated carriers in magnetic III–V semiconductor heterostructures of (In,Mn)As/ GaSb. Phys. Rev. Lett., 78: 4617-4620.

[3] Ohno, H. 1998. Making nonmagnetic semiconductors ferromagnetic. Science, 281: 951-956.

[4] Pearton, S.J., Heo, W.H., Ivill, M., Norton, D.P. and Steiner, T. 2004. Dilute magnetic semiconducting oxides. Semicond. Sci. Technol, 19: R59-R74.

[5] Zhang, H., Wang, N., Wang, S. and Zhang, Y. 2020. Effect of doping 3d transition metal (Fe, Co, and Ni) on the electronic, magnetic and optical properties of pentagonal ZnO_2 monolayer. Phys. E Low Dimens, Syst. Nanostructures, 117: 113806.

[6] Singh, P., Kumar, R. and Singh, R.K. 2019. Progress on transition metal-doped ZnO nanoparticles and its application. Ind. Eng. Chem. Res, 58: 17130-17163.

[7] Kittilstved, K.R., Norberg, N.S. and Gamelin, D.R. 2005. Chemical manipulation of high TC ferromagnetism in ZnO diluted magnetic semiconductors. Phys. Rev. Lett., 94:147209.

[8] Marquina, J., Quintero, E., Ruette, F. and Bentarcurt, Y. 2020. Theoretical study of Mn doping effects and O or Zn vacancies on the magnetic properties in wurtzite ZnO, Chin. J. Phys., 63: 63-69.
[9] Pan, H., Zhang, Y., Hu, Y. and Xie, H. 2020. Effect of cobalt doping on optical, magnetic and photocatalytic properties of ZnO nanoparticles. Optik, 208: 164560.
[10] Kayani, Z.N., Iram, S., Rafi, R., Riaz, S. and Naseem, S. 2018. Effect of Cu doping on the structural, magnetic and optical properties of ZnO thin films. Appl. Phys. A, 124:468.
[11] More, D., Phadnis, C., Basu, S., Pathak, A., Dubenko, I., Ali, N., Jha, S., Bhattachryya, D. and Mahamuni, S. 2014. Correlation of structural and magnetic properties of Ni-doped ZnO nanocrystals. J. Phys. D Appl. Phys., 47: 045308.
[12] Malaidurai, M., Santosh B.K. and Thangavel, R. 2019. Spin polarized carrier injection driven magneto-optical Kerr effect in Cr-doped ZnO nanorods. Phys. Lett. A, 383: 2988-2992.
[13] Yıldırım, Ö.A. and Durucan, C. 2016. Room temperature synthesis of Cu incorporated ZnO nanoparticles with room temperature ferromagnetic activity, Structural, optical and magnetic characterization. Ceram. Int., 42: 3229-3238.
[14] Wang, Q., Sun, Q., Chen, G., Kawazoe, Y. and Jena, P. 2008. Vacancy-induced magnetism in ZnO thin films and nanowires. Phys. Rev. B, 77: 205411.
[15] Luo, X., Zhang, Y., Mao, S.S. and Lin, L. 2006. Fabrication and characterization of ZnO nanowires based UV photodiodes. Sensors and Actuators A, 127: 201-206.
[16] Nomura, K., Ohta, H., Ueda, K., Kamiya, T., Hirano, M. and Hosono, H. 2003. Thin film transistor fabricated in single-crystalline transparent oxide semiconductor. Science, 300**:** 1269-1272.
[17] Bagnall, D.M., Chen, Y.F., Zhu, Z., Yao, T., Koyama, S., Shen, M.Y. and Goto, T. 1997. Optically pumped lasing of ZnO at room temperature. Appl. Phys. Lett., 70**:** 2230.
[18] Plugaru, R. and Plugaru, N. 2016. Assessment of structural, optical and conduction properties of ZnO thin films in the presence of acceptor impurities. J. Phys.: Condens. Matter, 28**:** 224008.
[19] Zhang, S. and Cao, Q. 2013. First-principles and experimental studies of the IR emissivity of Sn-doped ZnO. Mat. Sci. Semicon. Proc., 16**:** 1447- 1453.
[20] Kelly, L.L., Racke, D.A., Schulz, P., Li, H., Winget, P., Kim, H., Ndione, P., Sigdel, A.K., Br´*e*das, J.-L., Berry, J.J., Graham, S. and Monti, O.L.A. 2016. Spectroscopy and control of near-surface defects in conductive thin film ZnO. J. Phys.: Condens. Matter, 28: 094007.
[21] Ahmad, I., Mazhar, M.E., Usmani, M.N., Mehmood, M., Abbas, W., Akhtar, N. and Ahmed, E. 2019. Auto-combustion synthesis of pure and Er, Dy co-doped ZnO nanomaterials for efficient methyl orange degradation using solar and visible light photocatalysis, Mater. Res. Express, 6: 075044.
[22] Sahoo, T., Kim, M., Baek, J H., Jeon, S.-R., Kim, J.S., Yu, Y.-T., Lee, C.-R. and Lee, I.-H. 2011. Synthesis and characterization of porous ZnO nanoparticles by hydrothermal treatment of as pure aqueous precursor, Mater. Res. Bull., 46**:** 525-530.
[23] Damonte, L.C., Z´ *e*lis, L.A.M., Soucase, B.M. and Fenollosa, M.A.H. 2004. Nanoparticles of ZnO obtained by mechanical milling. Powder Technol,, 148: 15-19.
[24] Risti´c, M., Musi´c, S., Ivanda, M. and Popovic, S. 2005. Solgel synthesis and characterization of nanocrystalline ZnO powder. J. Alloy Compd., 397: L1-L4.
[25] Hjiri, M., El Mir, L., Leonardi, S.G., Pistone, A., Mavilia, L. and Neri, G. 2014. Al doped ZnO for highly sensitive CO gas sensors. Sens. Actuators B Chem., 196: 413-420.
[26] Ovhal, M.M., Kumar, A.S., Khullar, P., Kumar, M. and Abhyankar, A.C. 2017. Photoluminescence quenching and enhanced spin relaxation in Fe doped ZnO nanoparticles. Mater. Chem. Phys., 195: 58-66.
[27] Ganesh, R.S., Durgadevi, E., Navaneethan, M., Patil, V.L., Ponnusamy, S., Muthamizhchelvan, C., Kawasaki, S., Patil, P.S. and Hayakawa, Y. 2017. Low temperature ammonia gas sensor based on Mn-doped ZnO nanoparticle decorated microspheres. J. Alloys Compd., 721: 182-190.
[28] Gacic, M., Jakob, G., Herbort, C. and Adrian, H. 2007, Magnetism of Co-doped ZnO thin films, Phys. Rev. B, 75: 205206.
[29] Henne, B., Ney, V., Lumetzberger, J., Ollefs, K., Wilhelm, F., Rogalev, A. and Ney, A. 2017. Local structure and magnetism of Co^{3+} in wurtzite Co: ZnO, Phys. Rev. B, 95: 054406.
[30] Herng, T.S., Qi, D.-C., Berlijn, T., Yi, J.B., Yang, K.S., Dai, Y., Feng, Y. P., Santoso, I., Hanke, A.S., Gao, X.Y., Andrew, T.S. W., Ku, W., Ding, J. and Rusydi, A. 2010. Room-Temperature Ferromagnetism of Cu-Doped ZnO Films Probed by Soft X-Ray Magnetic Circular Dichroism. Phys. Rev. Let., 105**:** 207201.
[31] Muthukumaran, S. and Gopalakrishnan, R. 2012. Structural, FTIR and photoluminescence studies of Cu doped ZnO nanopowders by Co-precipitation method. Opt. Mater., 34: 1946-1953.
[32] Daratika, D.A. and Baqiya, M.A. 2017. Darminto, Synthesis of Zn1-*x*Cu*x*O nanoparticles by coprecipitation and their structure and electrical Property, IOP Conf. Ser. Mater. Sci. Eng., 196: 012009.
[33] Elilarassi, R. and Chandrasekaran, G. 2010. Structural, optical and magnetic characterization of Cu-doped ZnO nanoparticles synthesized using solid state reaction method. J. Mater. Sci.: Mater Electron, 21: 1168- 1173.
[34] Phoohinkong, W., Foophow, T. and Pecharapa, W. 2017. Synthesis and characterization of copper zinc oxide nanoparticles obtained via metathesis process. Adv. Nano. Sci.: Nanosci. Nanotechnol, 8: 035003.
[35] Wang, Z., Xiao, W., Tian, M., Qin, N., Shi, H., Zhang, X., Zha, W., Tao, J. and Tian, J. 2020. Effects of Copper Dopants on the Magnetic Property of Lightly Cu-Doped ZnO Nanocrystals. Nanomaterials, 10 (8): 1578.
[36] Toby, B.H. 2006. R factors in Rietveld analysis: how good is good enough?. Powder Diffr., 21: 67-70.
[37] Kisi, E.H. and Elcombe, M.M. 1989. u parameters for the wurtzite structure of ZnS and ZnO using powder neutron diffraction. Acta Crystallogr Sec. C, 45: 1867-1870.
[38] Shannon, R. 1976. Revised effective ionic radii and systematic studies of interatomic distances in halides and chalcogenides. Acta Crystallogr. Sec. A, 32: 751-767.

[39] Zhang, Z., Yi, J.B., Ding, J., Wong, L.M., Seng, H.L., Wang, S.J., Tao, J.G., Li, G.P., Xing, G.Z., Sum, T.C., Huan, C.H.A. and Wu, T. 2008. Cu-doped ZnO nanoneedles and nanonails: morphological evolution and physical properties. J. Phys. Chem. C, 112: 9579-9585.
[40] Shukla, G. 2009. Magnetic and optical properties of epitaxial n-type Cu-doped ZnO thin films deposited on sapphire substrates. Appl. Phys. A, 97: 115-118.
[41] Khan, G.R. 2020. Crystallographic, structural and compositional parameters of Cu-ZnO nanocrystallites. Appl Phys A, 126(4): 311.
[42] Singhal, S., Kaur, J., Namgyal, T. and Sharma, R. 2012. Cu-doped ZnO nanoparticles: Synthesis, structural and electrical properties. Physica B, 407(8): 1223-1226.
[43] Ganesh, R.S., Durgadevi, E., Navaneethan, M., Patil, V.L.D., Ponnusamy, S., Muthamizhchelvan, C., Kawasaki, S., Patil, P.S. and Hayakawa, Y. 2018. Tuning the selectivity of NH_3 gas sensing response using Cu-doped ZnO nanostructures. Sensors Actuators A: Phys., 269(1): 331-341.
[44] Khokhra, R., Bharti, B., Lee, H.N. and Kumar, R. 2017. Visible and UV photo-detection in ZnO nanostructured thin films via simple tuning of solution method. Sci. Rep., 7: 15032.
[45] Mishra, D.K., Kumar, P., Sharma, M.K., Das, J., Singh, S.K., Roul, B.K., Varma, S., Chatterjee, R., Srinivasu, V.V. and Kanjilal, D. 2010. Ferromagnetism in ZnO single crystl. Physica B: Condens. Matter.
[46] Claros, M., Setka, M., Jimenez, Y.P. and Vallejos, S. 2020. AACVD synthesis and characterization of iron and copper oxides modified ZnO structured films. Nanomaterials, 10(3): 471.
[47] Vijayaprasath, G., Murugan, R., Mahalingam, T., Hayakawa, Y. and Ravi, G. 2015. Preparation of highly oriented Al: ZnO and Cu/Al: ZnO thin films by sol-gel method and their characterization. J. Alloy. Compd., 649: 275-284.
[48] Anbuselvan, D. and Muthukumaran, S. 2015. Defects related microstructure, optical and photoluminescence behavior of Ni, Cu co-doped ZnO nanoparticles by Co-precipitation method. Opt. Mater., 42: 124-131.
[49] Kuriakose, S., Satpati, B. and Mohapatra, S. 2015. Highly efficient photocatalytic degradation oforganic dyes by Cu doped ZnO nanostructures. Phys. Chem. Chem. Phys., 17: 25172.
[50] Lin, B. and Fua, Z. 2001. Green luminescent center in undoped zinc oxide films deposited on silicon substrates. Appl. Phys. Lett., 79: 943-945.
[51] Peng, X., Xu, J., Zang, H., Wang, B. and Wang, Z. 2008. Structural and PL properties of Cu-doped ZnO films. J. Lumin., 128(3): 297-300.
[52] Gao, T., Meng, G., Tian, Y., Sun, S., Liu, X. and Zhang, L. 2002. Photoluminescence of ZnO nanoparticles loaded into porous anodicalumina hosts. J. Phys.: Condens. Matter, 14(7): 12651-12656.
[53] Kwon, B.J., Kim, J.Y., Choi, S.M. and An, S.J. 2014. Highly transparent and conducting graphene-embedded ZnO films with enhanced photoluminescence fabricated by aerosol synthesis. Nanotechnology, 25: 085701.
[54] Dhara, S. and Giri, P.K. 2012. Improved fast photoresponse from Al doped ZnO nanowires network decorated with Au nanoparticles. Chem. Phys. Lett., 541: 39-43.
[55] Michea, C.R., Morel, M., Gracia, F., Morell, G. and Mosquera, E. 2020. Influence of copper doping on structural, morphological, optical, and vibrational properties of ZnO nanoparticles synthesized by sol gel method. Surf. Interfaces, 21: 100700.
[56] Anandan, S., Muthukumaran, S. and kumar, M.A. 2014. Structural and optical properties of Y, Cu co-doped ZnO nanoparticles by sol-gel method. Superlattices Microstruct, 74: 247-260.
[57] Bhardwaj, R., Bharti, A., Singh, J.P., Chae, K.H. and Goyal, N. 2020. Influence of Cu doping on the local electronic and magnetic properties of ZnO nanostructures. Nanoscale-Advanc.
[58] Suwanboon, S., Amornpitoksuk, P., Bangrak, P., Sukolrat, A. and Muensit, N. 2010. The dependence of optical properties on the morphology and defects of nanocrystalline ZnO powders and their antibacterial activity. J. Ceram. Process. Res., 11(5): 547-551.
[59] Sajjad, M., Ullaha, I., Khanb, M.I., Khanc, J., Khana, M.Y. and Qureshi, M.T. 2018. Structural and optical properties of pure and copper doped zinc oxide nanoparticles. Results Phys., 9: 1301–1309.